Adaptive torque control of friction stir welding for the purpose of estimating tool wear

B Gibson*, **G Cook, T Prater, W Longhurst, A M Strauss,** and **C D Cox**
Vanderbilt University, Nashville, Tennessee, USA

The manuscript was received on 28 May 2010 and was accepted after revision for publication on 11 October 2010.

DOI: 10.1177/2041297510393629

Abstract: In this paper, an adaptive torque controller for friction stir welding (FSW) that can estimate parameters such as probe radius which may be changing throughout the welding process is presented. Implementing an adaptive controller with this capability would be of interest to industry sectors in which FSW is performed on high melting point alloys or metal matrix composites (MMC). Welding these materials has shown a greatly accelerated rate of tool wear. Simulations were conducted to examine how extreme tool wear would affect controller performance and how accurately the controller could estimate the probe radius. A simplified wear model consisting of a linear decrease in probe radius was used to verify controller performance. Next, a wear model consistent with wear patterns seen in the welding of highly abrasive materials was developed. Results indicate that torque is controlled effectively while a change in system dynamics is experienced, as would be expected with adaptive control, but also that the tool profile is accurately estimated after an initial identification period.

Keywords: friction stir welding, torque, adaptive control, tool wear

1 INTRODUCTION

1.1 Friction stir welding

Friction stir welding (FSW) is a proven solid-state joining technique that was invented in 1991 at The Welding Institute of Cambridge, England [**1**]. FSW is currently employed in a wide range of industries, including aerospace, land transportation, railway, and marine. The advantages of FSW are numerous. This joining technique allows for the welding of dissimilar materials or materials that are difficult or impossible to fusion weld. In addition, FSW is an energy efficient process that requires no shielding gas or filler material. There are no fumes, arc flash, or spatter associated with the process, and the relatively low temperatures result in low distortion and low residual stresses [**2**].

**Corresponding author: Vanderbilt University, 2301 Vanderbilt Place, PMB 351592, Nashville, TN 37235-1592, USA.*
email: brian.t.gibson@vanderbilt.edu

The welding process involves a non-consumable rotating tool, consisting of a probe and shoulder, which traverses the joint line of materials to be joined. Figure 1 displays the FSW process. The process employs three basic phenomena: heating, plastic deformation, and forging [**3**]. Heat is generated through both friction and plastic deformation of the welded material. FSW has been performed on a variety of joint configurations, including butt joints, lap joints, and T-joints [**4**]. A number of tool designs have been tested and optimized to maximize material flow and interrupt oxide layers at the interface of the materials [**5**]. Tools typically have threaded cylindrical probes; however, probes may take other forms with asymmetrical geometry. Shoulders are often scrolled to enhance the material containment ability of the tool.

1.2 Tool wear

Wear is also of concern in the area of tool design. Steel tools are commonly used for the welding of low

melting-point alloys such as aluminum. Steel becomes inadequate, however, when more abrasive materials, such as metal matrix composites (MMC), are welded. The abrasive nature of the imbedded particles leads to greatly accelerated tool wear [**4**, **6**]. Figure 2 displays the progressive nature of tool wear on MMC.

Tool wear can potentially alter the material flows within the weld seam [**7**]. It would not be unusual for tools that have experienced significant wear to produce less than adequate vertical flows, which can lead to voids that run the length of the weld [**6**]. Figure 3 displays cross-sections of welds performed with highly worn or 'self-optimized' tool geometry.

Statistical models have been developed at Vanderbilt University to predict the volume percentage of tool wear that will occur based on weld parameters. In a study by Prater *et al.* [**8**], a formula was developed through statistical analysis that predicts the amount of wear on a steel trivex tool while welding MMC (Al 359/SiC/20P). The percentage tool wear is given by [**8**]

$$W = 0.584(l) - 1.038(v) + 0.009(w) - 6.028$$

where W is the percentage tool wear, l is the weld length in inches, v is the traverse rate in inches/min, and ω is the tool rotation speed in r/min. The model was tested against experimental results over a range of welding parameters and produced a maximum error of only 13.4 per cent.

While these types of models are valuable for predicting the amount of wear that may take place over a given weld, it is more desirable to have an in-process prediction of tool wear based on force and/or torque feedback signals. An estimate of this type is more likely to produce an accurate picture of the amount of wear that is taking place at a given time.

1.3 Force and torque control

The forces and torque experienced by a FSW tool during welding can vary greatly depending on the welded material, tool geometry, joint configuration, and weld parameters. The axial force (F_z) is most significant and can range in values from 1 to 15 kN for aluminum welds [**2**]. Torque values, which strongly depend on tool design and weld parameters, can be as high as 60 Nm [**9**]. Planar forces are often measured for research purposes as well. These forces are the traversing force (F_x) and the side force (F_y), and they are usually much lower in magnitude when compared to the axial force. Because FSW is often

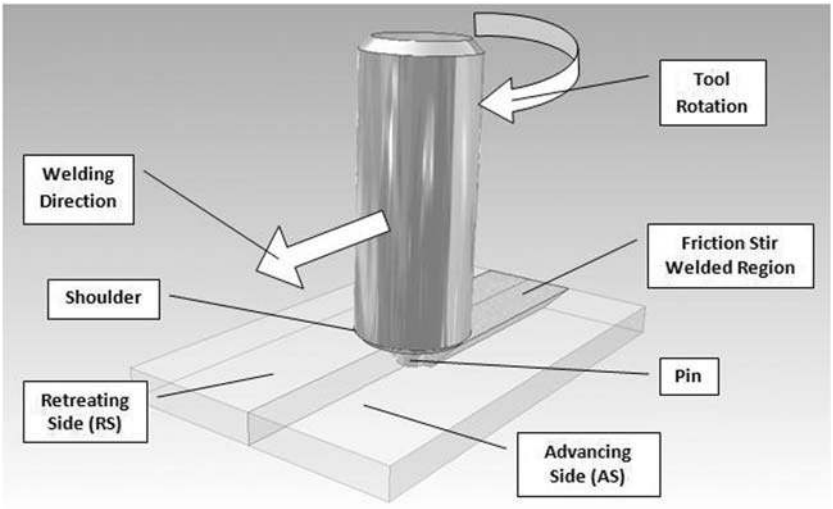

Fig. 1 FSW process

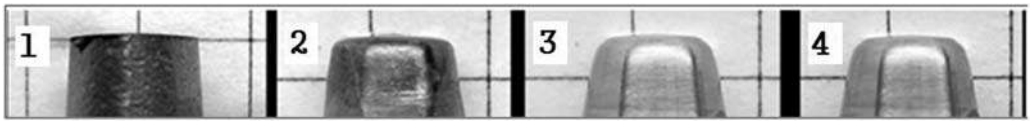

Fig. 2 Progressive tool wear on MMC at 2000 r/min, 7 inches/min: (1) new probe; (2) 8 inches of weld; (3) 16 inches of weld; and (4) 24 inches of weld

performed at the end of compliant industrial robots and on materials that may exhibit significant thickness variations, it is usually necessary to employ some type of force control, torque control, or a hybrid control to limit loads on the robot joints and links and to keep the tool properly engaged with the material surface [**10**].

To account for the compliant nature of industrial robots and material variation, force control with plunge depth as the controlling variable or torque control with plunge depth as the controlling variable are most commonly used. Force and torque control have proved to be advantageous in other ways, as well. When force control is used with rotation speed as the controlling variable, increased weld strength can be achieved. When force control is used with traverse speed as the controlling variable, heat distribution or weld input energy along the weld seam can be controlled [**3**]. Longhurst *et al.* [**11**] used a PID control architecture tuned with the Ziegler–Nichols method to successfully implement torque control in FSW. Implementing adaptive torque control in FSW will allow the welding process to be referenced to a model, which will allow for the estimation of in-process weld parameters, including tool profile.

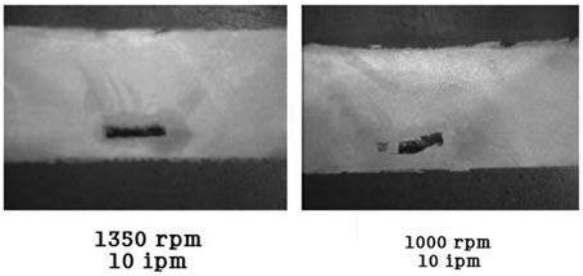

Fig. 3 Weld defects resulting from worn trivex tool

2 CONTROLLER DESIGN

2.1 Overall control concept

A conceptual flowchart for controlling torque and estimating tool wear is shown in Fig. 4. Weld parameters that are used in the simulation of FSW are also fed into the adaptive torque controller and process model. This is where tool wear estimates are produced, based on a comparison of the model and the actual process. The model-based partitioned controller was developed using Craig's method [**12**]. Craig's method has been used successfully in other industrial applications, such as adaptive voltage control in arc welding [**13**].

2.2 Adaptive control concept

In FSW, the torque experienced by the tool depends on, among other factors, plunge depth. Therefore, traditionally, plunge depth is changed to maintain a constant desired torque value during steady-state welding (not during tool plunge or tool retraction). When extreme tool wear is experienced, the relationship between plunge depth and torque is not fixed. To implement adaptive control, a process constant, K_{pt}, is introduced to the control loop. K_{pt} is a variable gain that changes with tool wear. The torque control loop may be seen in Fig. 5.

2.3 Design of adaptive control system

The transfer function of the servo motor controlling tool plunge has been adapted from a study by Longhurst [**3**] and simplified so it can be applied to an adaptive controller using Craig's method [**12**]. The transfer function is given by

$$G_s(s) = \frac{P}{T_m} = \frac{K_s}{s(s + 0.25)} \tag{1}$$

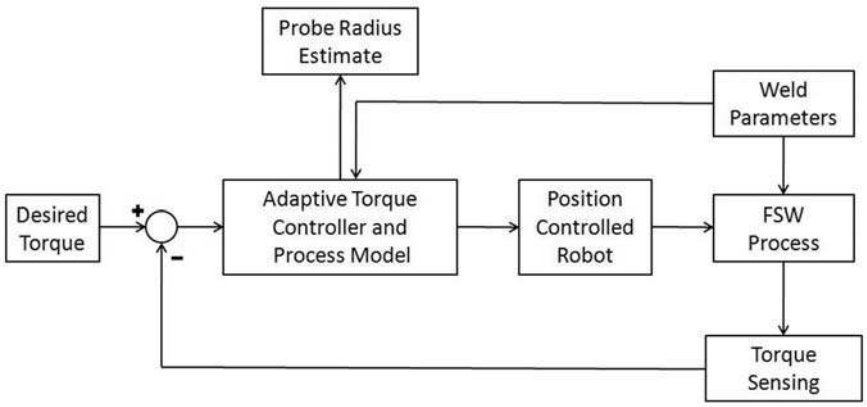

Fig. 4 Adaptive control flowchart

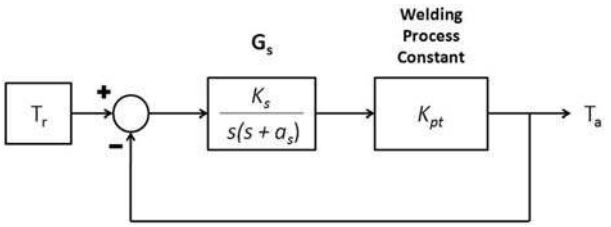

Fig. 5 Closed loop torque control

where P represents position and T_m represents motor torque. If $P * K_{pt} = T_a$ is used in equation (1), the differential equation may be written as

$$\ddot{T}_a + 0.25\dot{T}_a = K_s K_{pt} T_m \tag{2}$$

Equation (2) may be rewritten in the form

$$\frac{1}{K_s K_{pt}}\ddot{T}_a + \frac{0.25}{K_s K_{pt}}\dot{T}_a = T_m \tag{3}$$

Equation (3) reveals that $C_1 = 0.25/K_s K_{pt}$ and $C_2 = 1/K_s K_{pt}$. Equation (3) may be rewritten

$$C_2\ddot{T}_a + C_1\dot{T}_a = T_m \tag{4}$$

Equation (4) is a non-linear second-order differential equation because C_1 and C_2 vary inversely with K_{pt}, which changes non-linearly with probe radius.

The adaptive controller is partitioned into a model-based portion and a servo portion. The control law for the model-based portion is

$$T_m = \alpha T'_m + \beta \tag{5}$$

Equating (4) and (5) yields

$$C_2\ddot{T}_a + C_1\dot{T}_a = \alpha T'_m + \beta \tag{6}$$

Parameters α and β must be chosen such that the system will appear as the linear second-order system

$$T'_m = \ddot{T}_a \tag{7}$$

To satisfy equations (6) and (7), α and β must be selected as

$$\alpha = C_2$$

$$\beta = C_1\dot{T}_a$$

The controller employs estimates of constants C_1 and C_2 that will be denoted $\hat{C}_1$ and $\hat{C}_2$. Parameter errors $\tilde{C}_1$ and $\tilde{C}_2$ will also be established that are $\tilde{C}_1 = C_1 - \hat{C}_1$ and $\tilde{C}_2 = C_2 - \hat{C}_2$. A proportional-plus-derivative control law is selected such that

$$T_m = \hat{C}_2\ddot{T}_a + \hat{C}_1\dot{T}_a \tag{8}$$

or

$$T_m = \hat{C}_2 T'_m + \hat{C}_1\dot{T}_a \tag{9}$$

where $T'_m = \ddot{T}_r + K_v\dot{e} + K_p e$ and $e = T_r - T_a$ with T_r representing the reference torque.

Equating (4) and (9) and substituting for T'_m yields

$$C_2\ddot{T}_a + C_1\dot{T}_a = \hat{C}_2\left[\ddot{T}_r + K_v\dot{e} + K_p e\right] + \hat{C}_1\dot{T}_a \tag{10}$$

The error equation can be realized by rearranging equation (10) as

$$C_2\ddot{T}_a + \left[C_1 - \hat{C}_1\right]\dot{T}_a = \hat{C}_2\ddot{T}_r + \hat{C}_2\left[K_v\dot{e} + K_p e\right]$$

then

$$\left[C_2 - \hat{C}_2\right]\ddot{T}_a + \left[C_1 - \hat{C}_1\right]\dot{T}_a = \hat{C}_2\left[\ddot{T}_r - \ddot{T}_a\right] + \hat{C}_2\left[K_v\dot{e} + K_p e\right]$$

finally

$$\tilde{C}_2\ddot{T}_a + \tilde{C}_1\dot{T}_a = \hat{C}_2\left[\ddot{e} + K_v\dot{e} + K_p e\right]$$

The error equation may be written as

$$\ddot{e} + K_v\dot{e} + K_p e = \frac{1}{\hat{C}_2}\left[\tilde{C}_2\ddot{T}_a + \tilde{C}_1\dot{T}_a\right] \tag{11}$$

Equation (11) may be written in matrix form as

$$\ddot{e} + K_v\dot{e} + K_p e = \frac{1}{\hat{C}_2}\mathbf{W}\left(\ddot{T}_a, \dot{T}_a\right)\boldsymbol{\Phi} \tag{12}$$

where $\mathbf{W}\left(\ddot{T}_a, \dot{T}_a\right) = \begin{bmatrix} \ddot{T}_a & \dot{T}_a \end{bmatrix}$ and $\boldsymbol{\Phi} = \begin{bmatrix} \tilde{C}_2 \\ \tilde{C}_1 \end{bmatrix}$.

The estimation of parameters C_1 and C_2 is driven by system error, or more specifically, the filtered servo error signal. The filtered servo error is given by

$$E_s(s) = (s + \psi)E(s) \tag{13}$$

When the Laplace transform of the error equation is substituted into equation (13), the result is

$$E_s(s) = \frac{s + \psi}{s^2 + K_v s + K_p}\left(\frac{1}{\hat{C}_2}W\left(\ddot{T}_a, \dot{T}_a\right)\Phi\right) \tag{14}$$

Assuming the strictly positive real lemma is satisfied, the state–space representation is

$$\begin{aligned} \dot{\boldsymbol{x}} &= \mathbf{A}\boldsymbol{x} + \mathbf{B}\left[\tfrac{1}{\hat{C}_2}\mathbf{W}\left(\ddot{T}_a, \dot{T}_a\right)\boldsymbol{\Phi}\right] \\ e_1 &= \mathbf{C}\boldsymbol{x} \end{aligned} \tag{15}$$

and

$$\boldsymbol{x} = \begin{bmatrix} e & \dot{e} \end{bmatrix}^{\mathrm{T}}$$

Also, matrices **P** and **Q** are positive definite such that $\mathbf{P} > 0$, $\mathbf{Q} > 0$, and

$$\begin{aligned} \mathbf{A}^{\mathrm{T}}\mathbf{P} + \mathbf{P}\mathbf{A} &= -\mathbf{Q} \\ \mathbf{P}\mathbf{B} &= \mathbf{C}^{\mathrm{T}} \end{aligned} \tag{16}$$

A Lyapunov function to ensure stability was selected as

$$v(\mathbf{x}, \boldsymbol{\Phi}) = \boldsymbol{x}^{\mathrm{T}}\mathbf{P}\boldsymbol{x} + \boldsymbol{\Phi}^{\mathrm{T}}\Gamma^{-1}\boldsymbol{\Phi} \tag{17}$$

the derivative of which is

$$\dot{v}(\boldsymbol{x}, \boldsymbol{\Phi}) = \dot{\boldsymbol{x}}^{\mathrm{T}}\mathbf{P}\boldsymbol{x} + \boldsymbol{x}^{\mathrm{T}}\mathbf{P}\dot{\boldsymbol{x}} + \dot{\boldsymbol{\Phi}}^{\mathrm{T}}\Gamma^{-1}\boldsymbol{\Phi} + \boldsymbol{\Phi}^{\mathrm{T}}\Gamma^{-1}\dot{\boldsymbol{\Phi}}$$

or

$$\dot{v}(\boldsymbol{x}, \boldsymbol{\Phi}) = -\dot{\boldsymbol{x}}^{\mathrm{T}}\mathbf{Q}\boldsymbol{x} + 2\dot{\boldsymbol{\Phi}}^{\mathrm{T}}\left(\mathbf{W}^{\mathrm{T}}\frac{1}{\widehat{C}_2}e_1 + \Gamma^{-1}\dot{\boldsymbol{\Phi}}\right) \tag{18}$$

where Γ is a diagonal matrix of estimator gains γ_1 and γ_2.

By choosing $\dot{\boldsymbol{\Phi}} = -\Gamma\mathbf{W}^{\mathrm{T}}\frac{1}{\widehat{C}_2}e_1$, the estimator equations become

$$\dot{\widehat{C}}_2 = \frac{\gamma_2 \ddot{T}_{\mathrm{a}}}{\widehat{C}_2}e_1$$

and

$$\dot{\widehat{C}}_1 = \frac{\gamma_1 \dot{T}_{\mathrm{a}}}{\widehat{C}_2}e_1 \tag{19}$$

The adaptive torque controller was constructed in MATLAB's Simulink. The Simulink model is shown in Fig. 6. Estimator equations (19) are implemented in the Adaptive Estimator block in the model. Estimates are fed into Alpha (α) and Beta (β) blocks which then form the control law (5). The Reference Torque block is a second-order filter whose input is a constant desired torque value with an added perturbation for adaptation purposes. The adaptation scheme is driven by error; therefore, a constant torque value alone would not allow the controller to adapt to changing system dynamics. The perturbation is a 1 Hz sine wave with an amplitude of 0.04. The FSW process is modelled in the Parameters block using Nunes's rotating plug model [**14**].

2.4 FSW model

In an experimental and theoretical study, Nunes *et al.* [**14**] developed a model for material flow in the FSW process. This model is known as the rotating plug model, and it is illustrated in Fig. 7. Nunes *et al.* [**14**] theorized that a thin layer of welded material sticks to, and rotates with, the probe. Immediately outside this thin layer of material is a narrow shear zone in which plastic deformation occurs. This constitutes the primary flow. Secondary material flows are created by threads on the probe, assuming a threaded probe is used. The torque on the tool may be determined by assuming it arises from the interactions between the rotating plug and the surrounding material. Also, it is assumed that the rotating plug is sufficiently thin such that it has the same dimensions as the probe. Torque arising from secondary flows is ignored to

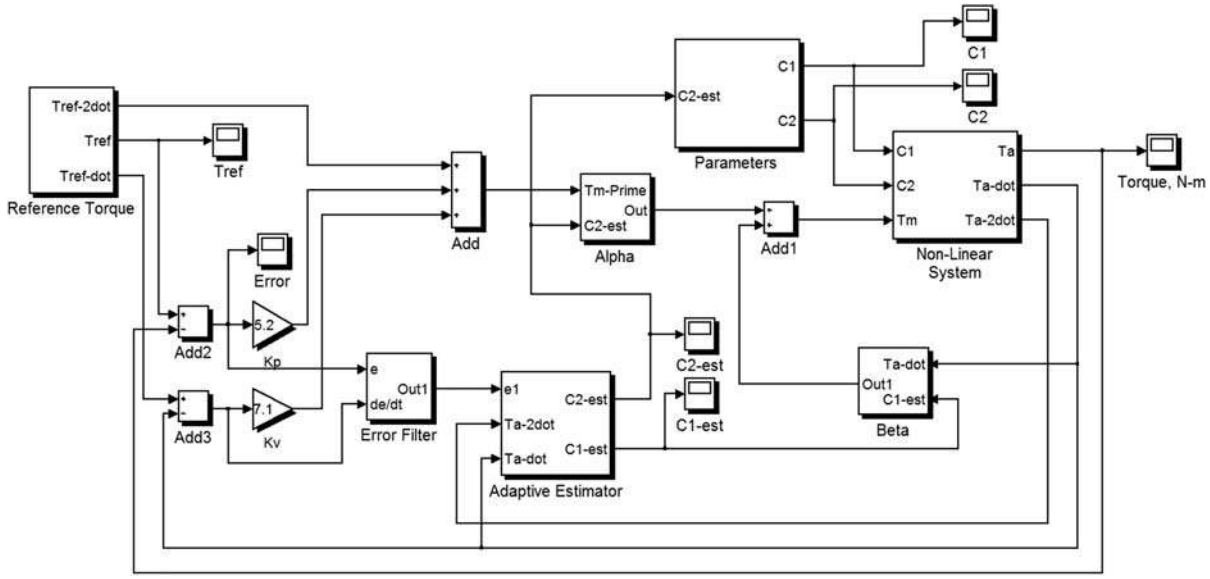

Fig. 6 Adaptive torque controller, Simulink model

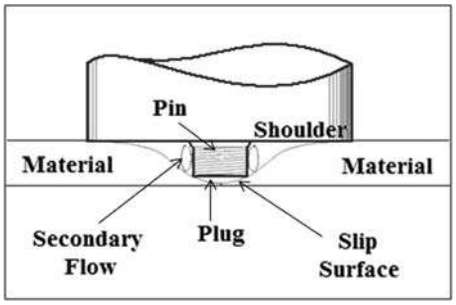

Fig. 7 Rotating plug model

allow for a simplified model. With these assumptions, the torque on the tool is given by [**14**]

$$T_{total} = T_{pin\ bottom} + T_{pin\ sides} + T_{shoulder}$$
$$T_{total} = \int_0^r 2\pi r^2 \sigma dr + 2\pi r^2 t\sigma + \int_0^R 2\pi r^2 \sigma dr \qquad (20)$$
$$T_{total} = \frac{2\pi R^3}{3}\left(1 + 3\frac{r^2 t}{R^3}\right)\sigma$$

where r is the probe radius, R is the shoulder radius, t is the probe depth, and σ is the shear flow stress. In their study, Nunes *et al.* [**14**] approximated the shear flow stress with

$$\sigma = \beta(T_{\mathrm{m}} - T)^2 \qquad (21)$$

in which T_{m} is the melting temperature of the welded material, T is the temperature at the shear zone, and β is a material constant. Also, the temperature at the shear zone is given by

$$T = 530^{\circ}\mathrm{C} - \sqrt{\frac{9765(T - 30^{\circ}\mathrm{C})}{RPM}} \qquad (22)$$

Nunes *et al.* [**14**] adjusted the constant, 9765, so that equation (22) would match experimental results.

In this research, the rotating plug model [**14**] has been used to simulate the FSW process in the Parameters block of the Simulink model in Fig. 6. The FSW process determines the variable gain K_{pt}, on which constants C_1 and C_2 depend. Initial welding parameters and materials were selected to align with the research of Nunes *et al.* [**14**] so that values of temperature and shear stress obtained from simulations could be confirmed with the experimental data collected in the Nunes study.

3 SIMULATION RESULTS

3.1 Welding simulation

Simulations in this research were designed to replicate extreme tool wear. A 2195 Al–Li material was selected to align with research performed by Nunes *et al.* [**14**]. For this material, $T_{\mathrm{m}} = 530\ ^{\circ}\mathrm{C}$ and $\beta = 0.26$ psi/K^2 [**15**]. A MMC material was not selected because the FSW model does not capture the effects of imbedded particles on torque. Tool rotation speed and traverse speed were selected as 700 r/min and 2 inches/min (50.8 mm/min), respectively. These welding parameters not only align with the research conducted by Nunes *et al.* [**14**] but also fall within the more restrictive operating envelope for particle reinforced materials defined by studies by Feng *et al.* [**16**] and Marzoli *et al.* [**17**]. Significant tool wear was simulated over the course of a single 8 inch (203.2 mm) sample weld, meaning the simulation time in Simulink was 240 s. The FSW tool used in the simulation featured a shoulder diameter of 0.75 inch (19.05 mm) and a cylindrical probe of 0.25 inch (6.35 mm) diameter and 0.25 inch (6.35 mm) length. The reference torque was selected as 21 Nm, which is slightly lower than the process torque indicated by the Nunes model for the selected parameters. This means that the controller will slightly retract the FSW tool to lower the torque to the desired level. It was necessary to select a lower desired torque because the Nunes model does not capture additional torque generated by the shoulder plunging below the surface of the material.

3.2 Controller tuning

The controller was tuned by simulating a step in probe radius at 120 s. The step change in radius is shown in Fig. 8. Using a step change is not representative of any type of phenomenon that would be seen in FSW, but rather an effective simulation to run for optimizing controller performance. Estimator gains, γ_1 and γ_2, and the error filter gain ψ were tuned so that estimates of C_1 and C_2 would adapt quickly with a relatively low amount of overshoot or undershoot. Figure 9 displays the estimates of parameters C_1 and C_2. After the tuning process was completed, the selected gains were $\gamma_1 = 1.7$, $\gamma_2 = 1.4$, and $\psi = 2$. Because it adapted faster than the estimate of C_1, the estimate of C_2 was selected to be used to derive the estimate of tool profile. C2-est was fed back to the FSW model in the Parameters block in Fig. 8 to be used to estimate tool profile.

3.3 Simulating uniform probe wear

A simple tool wear model was simulated by assuming a linear change in probe radius over the length of the weld. Experiments have shown that assuming a linear relationship between tool wear and distance traversed is valid, given particular rotation speeds

Fig. 8 Step change in probe radius for controller tuning purposes

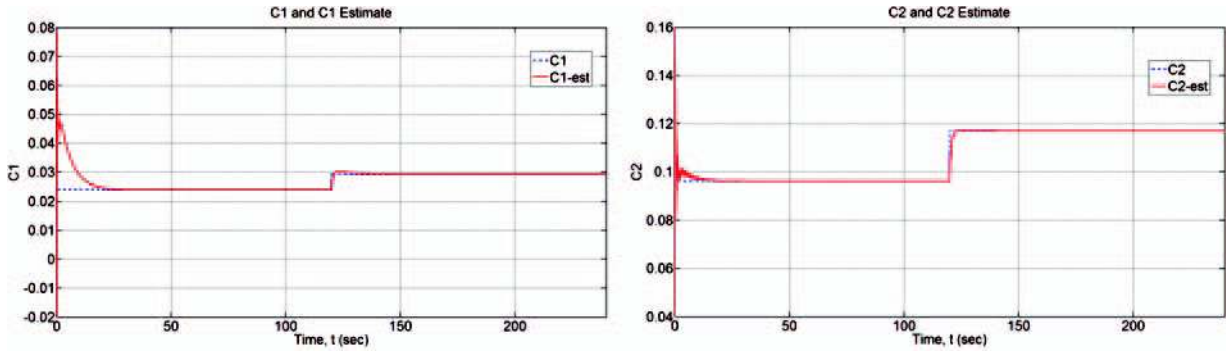

Fig. 9 Controller estimates with step change in probe radius

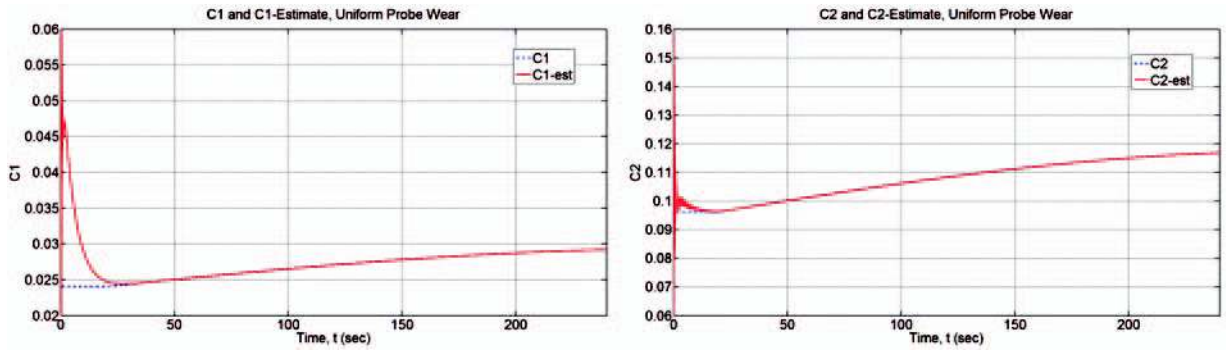

Fig. 10 Non-linear changes in controller parameters while simulating uniform probe wear

and traverse rates [**8**]. The linear decrease in probe radius began at 20 s and continued throughout the simulation. The linear change in probe radius created non-linear changes in parameters C_1 and C_2. Figure 10 shows how the controller identified and adapted to these non-linear changes. The adaptation scheme of the controller was used to estimate the probe radius. Figure 11 displays the actual change in probe radius and the controller estimate. After an initial identification period, the controller estimated the probe radius accurately while controlling torque with very low error.

Fig. 11 Estimation of uniform probe wear

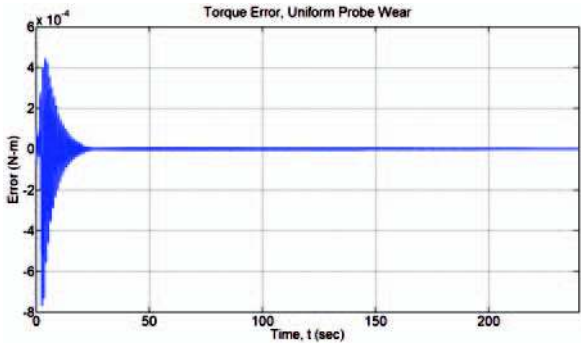

Fig. 12 Torque error while simulating uniform probe wear

Figure 12 shows the error in torque while uniform tool wear is simulated.

3.4 Simulating non-uniform probe wear

The uniform probe wear simulation proved that the adaptive controller not only controlled torque properly during FSW, but that it can also accurately identify welding parameters that are changing throughout the weld. The uniform probe wear model is not representative of wear modes that are seen in FSW however. In order to create a more realistic tool wear simulation, a wear model was developed that follows patterns seen in studies at Vanderbilt University. A change in probe radius was again simulated, but that change was correlated to a change in cross-sectional area of the probe. In studies of tool wear, cross-sectional area, which is proportional to volume, is most often used to characterize the wear patterns. The probe length was segmented into five regions, each of which constitutes 20 per cent of the initial cross-sectional area. Tool wear was simulated by governing, beginning at the start of the weld, the percentage that each region constitutes of the whole. These percentage values were matched to experimental data obtained by Prater *et al.* [**8**]. Figure 13 displays

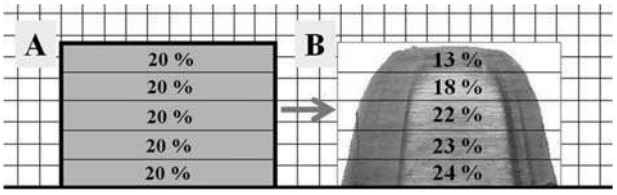

Fig. 13 Non-uniform tool wear model: (a) original probe; (b) probe after 24 inches of weld

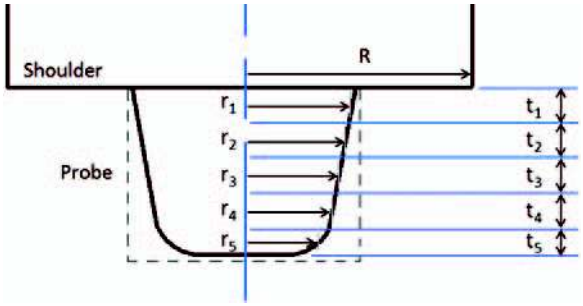

Fig. 14 Non-uniform probe wear model for radial estimation

the tool wear simulation model, which is based on a 24 inch (609.6 mm) MMC weld at 1500 r/min and 7 inches/min (177.8 mm/min). The cross-sectional percentages were determined using a digital image of the probe and the pixel count tool in a digital image software package. Other common methods for quantifying tool wear include microscopy, weighing, mechanical gauging, profilometry, and the use of radiotracers.

Because it is known how each region changes in size proportionately to one another, at any given time during the simulation the controller can estimate the average radius of the regions. Figure 14 shows a diagram of the average radii. A wear rate could also be predicted for t_5, which would represent wear in the axial direction.

To simulate tool wear using the newly developed non-uniform wear model, weld parameters in the simulation were changed to 1500 r/min and 7 inches/min (177.8 mm/min). To replicate a 24 inch (609.6 mm) weld, the simulation was run for 206 s. Total probe cross-sectional area was varied linearly from 4.032 E−5 to 3.34 E−5 m^2 to account for the 17.16 per cent decrease seen by Prater *et al.* [**8**], and the five regional cross-sectional area percentages were varied linearly from their initial values of 20 per cent to the new percentages shown in Figure 13. Figure 15 shows how the controller estimated the radius of each region.

Finally, the wear estimation output of the controller was configured to estimate the percentage tool

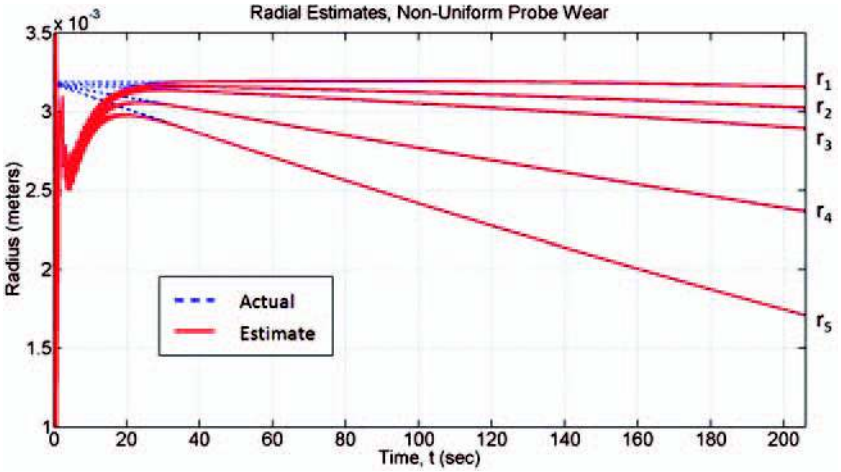

Fig. 15 Radial estimates while non-uniform tool wear is experienced

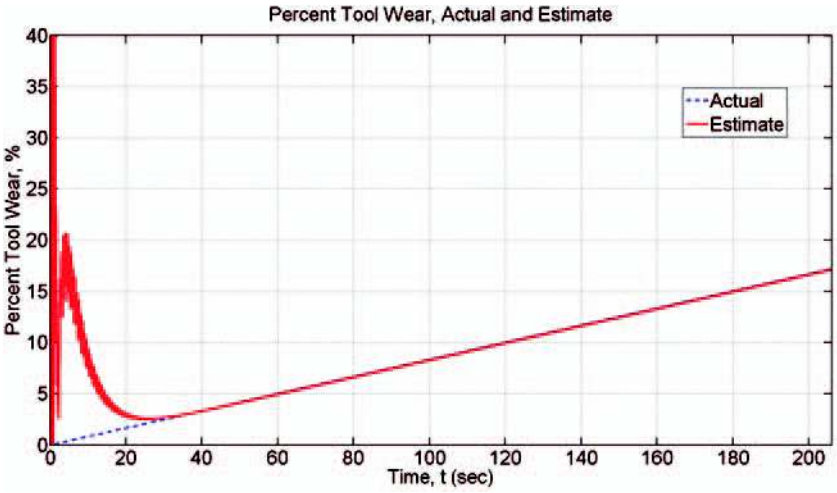

Fig. 16 Percentage tool wear estimation

wear based on cross-sectional area, which is the most common characterization of tool wear. Figure 16 shows the actual percentage tool wear and the controller estimate of the same. Figure 17 shows the error in the percentage tool wear estimation.

4 DISCUSSION AND CONCLUSIONS

The adaptive torque controller developed for estimating parameters during the FSW process was simulated using two different wear models. First, controller performance was tested by assuming a simple wear model, which involved uniform wear of the probe radius. Next, a non-uniform wear model was developed using the results of FSW experiments in which welding was performed on highly abrasive MMC. This model involved sectioning the probe into five regions and specifying how each region changed in relation to one another based on cross-sectional area. In both cases, the results were:

1. The controller adapted to the changing system dynamics caused by extreme tool wear and controlled torque with very low error.
2. The controller identified parameters that were changing throughout the weld, such as probe radius or probe cross-sectional area, after an initial identification period.

In the case of uniform probe wear, the controller accurately estimated the probe radius after 20 s. In the case of non-uniform probe wear, the controller accurately estimated the radii of all five regions after approximately 30 s. The percentage tool wear by area was accurately estimated after approximately 30 s as well. This means that for a traverse rate of 7 inches/min, as in the simulations, the controller can estimate

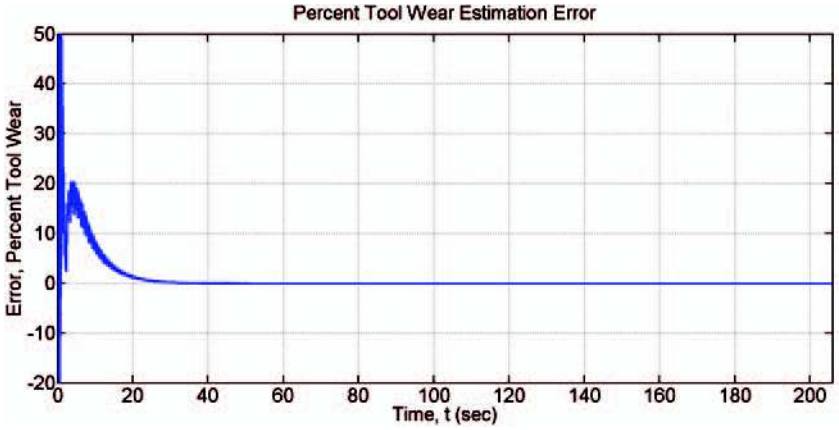

Fig. 17 Percentage tool wear estimation error

tool profile after approximately 3 to 4 inches of weld. For most industrial applications, this identification period would be sufficiently small.

Empirical models have been developed by Prater *et al.* [**8**] and others that are valuable in predicting the amount of tool wear that may take place over the course of a weld, given a particular rotation speed and traverse rate. While these models are extremely valuable in process planning, there are variables such as material variation of both the tool and the welded material that can reduce the accuracy of these models. Of greater value is knowledge of the actual amount of tool wear that has taken place at any point throughout the weld. The implementation of adaptive torque control allows for this capability. Figure 17 indicates that after approximately 30 s, there is zero error in the estimation of percentage tool wear.

Having an in-process estimate of tool wear may be especially useful when a tool is used that exhibits features such as threads on the probe. In most industrial applications of FSW, tool design and tool material are selected only after extensive testing to ensure any tool wear will not be detrimental to weld quality; however, tool features such as threads are often the weak link of tool design. The wear estimation capabilities of the adaptive torque controller would allow operators to know when tool features such as threads have experienced significant wear, which may lead to weld defects resulting from insufficient flows. Tool changes could therefore be performed when process feedback signals indicate they are needed, rather than on a set schedule. This could result in savings of both time and money for manufacturers who use FSW. Furthermore, because of the radial estimation capabilities displayed in Figure 15, is possible to know when during the process certain locations on the probe experience more wear than others. This may lead designers to create more robust tools that can handle the demands of custom industrial FSW applications.

Using adaptive torque control in FSW may prove to be advantageous in other ways as well. Although adaptive control may not be necessary for controlling torque during the steady-state welding process, it may prove to be useful for controlling torque during tool plunge or retraction, during which there are nonlinear phenomena that would necessitate adaptive control. Future work will focus on developing a model for thread wear prediction and implementing adaptive control of FSW at the Vanderbilt University Welding Automation Laboratory. Implementation will allow for the direct comparison of controller estimates to FSW tool measurements.

ACKNOWLEDGMENTS

This research was supported by the NASA Tennessee Space Grant Consortium.

REFERENCES

1 **Thomas, W. M., Nicholas, E. D., Needham, J. C., Church, M. G., Templesmith, P.,** and **Dawes, C. J.** *International Patent Application no. PCT/GB92/02203 and GB Patent Application no. 9125978.9,* 1991.
2 **Cook, G. E., Crawford, R., Clark, D. E.,** and **Strauss, A. M.** Robotic friction stir welding. *Industrial Robot: Int. J.*, 2004, **131**, 55–63.
3 **Longhurst, W. R.** Force control of friction stir welding. PhD *Dissertation*, 2009 (Vanderbilt University, USA).
4 **Mishra, R. S.** and **Ma, Z. Y.** Friction stir welding and processing. *Mater. Sci. Engng*, 2005, **50**, 1–78.
5 **Thomas, W. M., Johnson, K. I.,** and **Wiesner, C. S.** Friction stir welding – recent developments in tool and process technologies. *Adv. Engng Mater.*, 2003, **5**(7), 485–490.

6 **Prater, T.** An investigation into the friction stir welding of Al 6061 and Al 6061/SiC/17.5p using diamond coatings. MSc *Thesis*, 2008 (Vanderbilt University, USA).

7 **Fernandez, G. J.** and **Murr, L. E.** Characterization of tool wear and weld optimization in the friction-stir welding of cast aluminum 359+20% SiC metal matrix composite. *Mater. Characterization*, 2004, **52**, 65–75.

8 **Prater, T. J., Strauss, A. M., Cook, G. E., Machemehl, C., Sutton, P.,** and **Cox, C.** Statistical modeling and prediction of wear in friction stir welding of metal matrix composite (Al 359/SiC/20P). *J. Manufact. Technol. Res.*, 2010, **2**, 1–13.

9 **Crawford, R., Cook, G. E., Strauss, A. M.,** and **Hartman, D. A.** Modeling of friction stir welding for robotic implementation. *Int. J. Modelling, Identification Control*, 2006, **1**(2), 101–106.

10 **Longhurst, W. R., Strauss, A. M., Cook, G. E., Cox, C. D., Hendricks, C. E., Gibson, B. T.,** and **Duwant, Y. S.** Investigation of force controlled friction stir welding for manufacturing and automation. *Proc. IMechE, Part B: J. Engng Manufact.*, 2010, **224**, 937–949.

11 **Longhurst, W. R., Strauss, A. M., Cook, G. E.,** and **Fleming, P. A.** Torque control of friction stir welding for manufacturing and automation. *Int. J. Adv. Manufact. Technol.*, 2010, **51**, 905–913.

12 **Craig, J. J.** *Introduction to robotics: mechanics and control*, 3rd ed, 2005, pp. 290–312 (Pearson Prentice Hall, Upper Saddle River, New Jersey, USA).

13 **Koseeyaporn, P., Cook, G. E.,** and **Strauss, A. M.** Adaptive voltage control in fusion arc welding. *IEEE Trans. Industr. Applic.*, 2000, **36**(5), 1300–1307.

14 **Nunes, A. C., Bernstein, E. L.,** and **McClure, J. C.** A rotating plug model for friction stir welding. *Presented at 81st American Welding Society Annual Convention*, 2000, Las Vegas, NV, USA.

15 **Talia, J. E.** and **Nunes, A. C.** Cracking during welding of 2195 Aluminum-Lithium alloy: Experimental approaches towards mechanism. In *Aluminum-Lithium Alloys for Aerospace Workshop*. NASA Conference Publication 3287, 1994, Marshall Space Flight Center, Huntsville, AL, USA.

16 **Feng, A. H., Xiao, B. I.,** and **Ma, Z. Y.** Effect of microstructural evolution on mechanical properties of friction stir welded AA2009/SiCp composite. *Composites Sci. Technol.*, 2008, **68**, 2141–2148.

17 **Marzoli, L. M., Strombeck, A. V., Dos Santos, J. F., Gambaro, C.,** and **Volpone, L. M.** Friction stir welding of an AA6061/Al_2O_{3p} reinforced alloy. *Composites Sci. Technol.*, 2006, **66**, 363–371.

APPENDIX

Notations

l	weld length
r	probe radius
R	shoulder radius
t	probe depth
T	shear zone temperature
T_m	melting temperature
ν	traverse rate (inches/min)
ω	tool rotation rate, r/min
W	percentage tool wear
σ	shear flow stress